

# Investigation of the Impact of Surface Roughness, on a Ship's Drag (Hull Resistance)

**Zainab Ali, Gabriella Bognár**

University of Miskolc, Institute of Machine and Product Design, Egyetemváros,  
3515 Miskolc, Hungary, e-mail: zainab.ali@student.uni-miskolc.hu,  
gabriella.v.bognar@uni-miskolc.hu

---

*Abstract: Recently, there has been an increasing focus on maritime transport, as it offers many advantages in terms of storage and transport. As a result, shipping companies need to reduce the fuel consumption of their vessels. These companies have tried to define methods of operation and maintenance in order to reduce greenhouse gas emissions and also to reduce operating costs, thus increasing company profits. One important parameter that directly affects speed, power requirements, and fuel consumption is the hull resistance. Computational Fluid Dynamics (CFD) can be used to calculate the resistance of a rough surface using special wall functions that take into account the effect of roughness on the boundary layer near the hull. These results can be compared with those of a smooth surface. In addition to the effect of surface roughness on hull resistance to pressure, this method also allows the combination of roughness and non-linear effects such as the spatial distribution of contaminants, the movement of the ship in waves, and the effect of thrust on hull resistance. Accordingly, the aim of this research is to determine the effect of surface roughness on the ship resistance for different values of roughness height, boundary layer, and values of velocity, pressure, and kinetic energy fields for the KVLCC2 model hull by CFD using the RANS equations and the  $k-\omega$  SST model. A numerical study was performed to determine how surface roughness affects the velocity field and kinetic energy.*

---

*Keywords: KVLCC2; ship hull roughness; velocity; pressure; kinetic energy; CFD;  $k-\omega$ SST*

---

## 1 Introduction

When the design and calculations for a ship, one of the most important things is to know the conditions under which the propeller will operate, such as the speed, pressure, kinetic energy and vortices. This is a very important parameter for predicting the thrust that the propeller can produce. Accordingly, the effect of the surface roughness on these two fields, in the working plane of the propeller, should be investigated. It is, therefore, necessary to understand and analyze the variations of the boundary layer around the ship, during motion, as this is the most important factor for studying the flow around the hull.

Prandtl [1] and Prandtl [2] defined the concept of a boundary layer as a thin zone near the surface of a body in a flowing fluid. A proper description of the physical processes taking place in the boundary layer between a fluid and a solid play an important role in fluid mechanics problems.

One of the foremost considerations in ship design and calculation, involves acquiring comprehensive knowledge about the propeller's operational conditions, encompassing factors such as velocity, pressure, kinetic energy, and vortices. The velocity field and kinetic energy levels at which the propeller functions assume the utmost significance in estimating the resultant thrust force. Consequently, it becomes imperative to investigate the influence of surface roughness on these two fields within the operational plane of the propeller. Thus, comprehending and scrutinizing the boundary layer that develops around the ship during its motion becomes pivotal, as it represents the principal determinant in studying the flow dynamics encircling the ship's hull.

Recently, several papers have been published on the analysis of the effect of surface roughness on flow parameters. Song *et al.* [3] conducted a numerical study on the effect of heterogeneous hull roughness on ship resistance and developed a URANS-based CFD model using the modified wall function approach. The predicted total resistance coefficients for different hull conditions were compared with experimental data from Song *et al.* [4] which showed a convincing agreement, where the highest error was around 6.1% for  $C_T$  of the Wigley hull with  $1/4$  bow-rough and  $1/4$  aft-rough conditions.

Similar observations were made by Song *et al.* [4] who related observations on the effects of heterogeneous hull roughness to the distribution of local wall shear stress and the roughness Reynolds number. The results showed that local differences in wall shear stress led to different roughness Reynolds numbers and hence different roughness effects depending on the location of hull roughness. The hypothesis of Song *et al.* [4] was confirmed in this study. Consequently, the numerical approach presented in this study can be applied to predict the effect of heterogeneous roughness on propeller propellers.

Reynolds Averaged Navier-Stokes (RANS) solvers, once developed only to evaluate the resistance of still water, have become increasingly complex, and the current generation now has unsteady-state capabilities. Shortly, the same numerical solver will be able to address problems of drag, sea-keeping, and maneuvering. CFD workshops on numerical ship hydrodynamics have been organized regularly since 1980 to assess the current state of CFD development and to set new goals [5].

In their paper, Tahara *et al.* [6] provided an overview of numerical methods and presented and discussed the results of traction and self-propulsion models of KRISO Container Ship (KCS), including a comparison with available experimental fluid dynamics (EFD) data. For the CFD model of a towed flat plate and a KRISO container ship (KCS) was prepared. In the wall function of the CFD model, the

roughness function of a previously created sand-grained surface was used to reproduce the roughness effect in the turbulent boundary layer. The output of the CFD simulations was then compared with the experimental results. The results showed a convincing agreement, in the case of the hull wave profile without the propeller, the maximum error observed was approximately 8%, indicating that the CFD approach accurately predicts the effect of roughness on the overall drag of the 3D hull. Finally, the effect of roughness on the different resistance components of the ship was investigated. The further evaluation took place at the CFD Workshop 2005 discussions in Tokyo, where both methods were presented.

This paper aims to analyze and interpret the variation of velocity, pressure, kinetic energy, and vorticity with surface roughness, which affect the operation of the propeller, by numerical simulation. The numerical calculations are performed by CFD with the choice of surface roughness function using the turbulent model for KRISO Very Large Crude Carrier no. 2 (KVLCC2) ship model.

## 2 Wall Functions

The large gradients in velocity, pressure, and kinetic energy can be handled in CFD either by direct solution or by using wall functions. Numerous experiments have been carried out to study and determine the properties of turbulent flows, particularly in the boundary layer, and these experiments have shown that the dimensionless curve of the velocity distribution ( $y^+, U^+$ ) can be described by a nearly identical formula in all cases, (see Fig. 1).

In the turbulent boundary layer, the hydrodynamic effects can be expressed by the non-dimensional mean velocity profile [8], [9]

$$y^+ = f(U^+) \quad (1)$$

where  $U^+$  is the non-dimensional velocity profile in the boundary layer,  $y^+$  is the non-dimensional distance measured perpendicular to the surface. These parameters are defined according to the following two equations

$$U^+ = \frac{U}{U_\tau} \quad (2)$$

$$y^+ = \frac{yU_\tau}{\nu} \quad (3)$$

where  $U$  is the average fluid velocity,  $U_\tau$  the frictional velocity is defined by the relation  $\sqrt{\tau_w/\rho}$ ,  $y$  the wall distance,  $\nu$  the kinematic viscosity,  $\tau_w$  the shear stress at the wall,  $\rho$  the fluid density.

The range  $0 < y^+ < 5$  is the linear range, where the effect of viscosity dominates and the equation  $U^+ = y^+$  is satisfied. In the range  $5 \leq y^+ \leq 70$ , the hybrid region, a transition from a linear relationship between  $U^+$  and  $y^+$  to a logarithmic relationship occurs. Within the range  $5 \leq y^+ \leq 30$ , both viscous and turbulent stresses are in equilibrium, and the linear relationship between  $U^+$  and  $y^+$  is preserved. At  $y^+ = 30$ , the logarithmic range in which the dominance of turbulence is satisfied begins, and the velocity distribution from this value is given as described in [7].

$$U^+(y^+) = \frac{1}{k_{const}} \ln y^+ + B; \quad 5 \leq y^+ \leq 30 \quad (4)$$

where  $B$  is a constant that considers the effect of surface roughness on the velocity distribution, and according to many experiments, the value  $B = 5$  is the best value for it and  $k_{const} = 0.41$  is Kármán's constant [10].

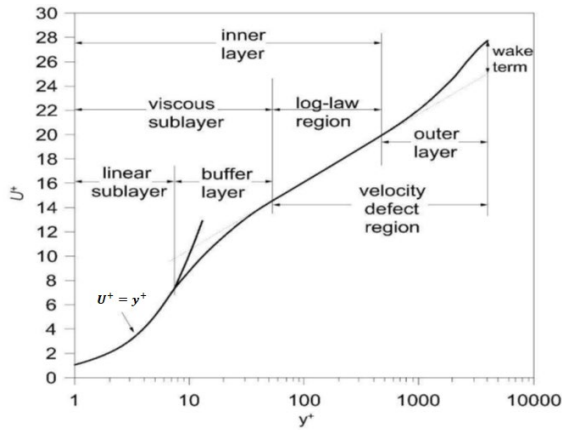


Figure 1

The non-dimensional curve of the velocity distribution in the turbulent boundary layer [7]

Surface roughness causes an increase in turbulence, which increases shear stresses at the wall and turbulence stresses, both of which reduce velocity. Roughness can be broadly divided into  $k$ -type and  $d$ -type roughness, which are the two most common types. This categorization is determined by the roughness functions used.

The primary parameter for the  $k$ -type roughness functions is the roughness height  $k$ , while the primary parameter for the  $d$ -type roughness functions is the pipe diameter [10]. Research on how surface roughness affects the turbulent boundary layer near the surface is of fundamental importance and has been studied since 1993 and is still ongoing, and the most important studies in this area, which we recommend the reader to review, include [10-20]. In this paper, we consider the roughness of  $k$ -type, since it has been shown that hull roughness is of  $k$ -type [21], and henceforth the term roughness is used to mean roughness of type  $k$ . In addition to other factors that may be used to determine roughness, the primary parameter is the roughness height  $k$  or the roughness height of equivalent sand  $k_s$ . The Reynolds number for roughness, which is a non-dimensional quantity, can take the place of the roughness height, and it is given by the following relationship see [21] [22]

$$k^+ = \frac{kU_\tau}{\nu} \quad (5)$$

The type of flow on the surface is defined according to the Reynolds number of roughness, according to this classification there are three types of flow regimes, the transiently rough regime, the fully rough regime, and the hydraulically smooth regime.

Although the same Reynolds number of roughness is recorded, it should be remembered that different types of roughness may produce different flow regimes on the surfaces [23]. For example, Schlichting [24] stated that if the surface roughness is isotropic sand grains and the value of  $k^+ < 5$ , then the prevailing flow regime is of the soft hydraulic type, and it turns into the coarse transitional in the range of values  $5 \leq y^+ \leq 70$ , and becomes fully coarse (the coarse and fully developed regime) when  $k^+ > 70$ .

Extending Nikuradse's research from 1933 [25], Schlichting used the following equations to depict the velocity profile in the turbulent boundary layer of the rough tube [24]

$$\frac{U_p U^*}{\tau_w / \rho} = \frac{1}{k} \ln \left( E \frac{U^+ y_p}{\mu} \right) - \Delta B; \quad U^+ = C_\mu^{1/4} k^{1/2}, \quad (6)$$

$$\Delta B = \frac{1}{k} \ln f_r U_p$$

$$U^+ = \frac{1}{k_{const}} \ln \left( \frac{y}{k_s} \right) + B_2 \quad (7)$$

where  $k_{const} = 0.41$  and the coefficients  $B_1, B_2$  have various values for various flow regimes.

From the above it can be observed how roughness affects the flow in the velocity profile, where it causes a decrease in the velocity diagram in the logarithmic domain, this decrease is called the roughness function, and  $\Delta U^+$ .

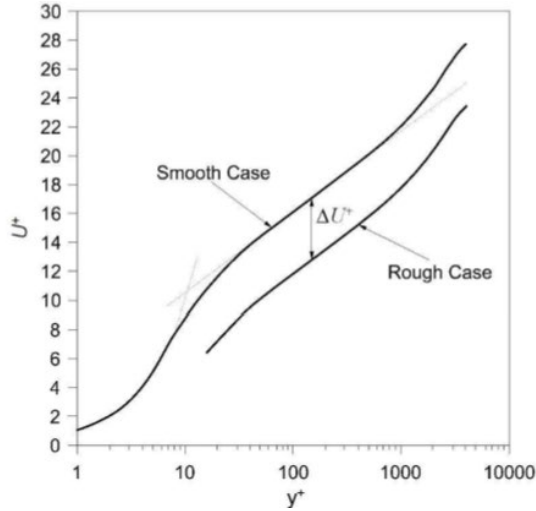


Figure 2

The effect of roughness on the velocity profile in the boundary layer region [10]

As has been previously demonstrated, the velocity profile region of the boundary layer region is where surface roughness has the greatest impact on the flow [9]. The surface roughness causes the region of complete perturbation to shift  $\Delta U^+$  (log-law region) downward in the  $(y^+, U^+)$  plot, see Fig. 2. As a result of these roughness-related variations in the velocity profile in the boundary layer region, frictional resistance increases [27] and the velocity profile, in this case, is given by the Eq. (8)

$$U^+ = \frac{1}{k} \ln(y^+) + B - \Delta U^+ \quad (8)$$

where  $\Delta U^+$  is the velocity obtained in a profile due to the roughness (velocity profile). By eliminating the expression  $\Delta U^+$  from the function provided by the equation, it is possible to represent the roughness velocity profile Eq. (1) and in the case of a smooth surface, it represents the velocity profile.

It is important to keep in mind that  $\Delta U^+$  simply disappears from Eq. (8) and this equation is transformed into Eq. (4) in the case of a smooth (without roughness) surface. Since there is no single roughness function that accounts for all types of roughness, the values of  $\Delta U^+$  are often determined empirically.

Here, it must be noted, that the wall function proposed by Demirel et al. [27] considered the effect of both coating and fouling. This wall function has been used in several reference studies, including but not limited to the study by Owen et al [28], where this function was used to investigate how performance is affected by surface roughness caused by coating and contamination. The results were very convincing. (The error in open water efficiency compared to the experimental result is 1.93%).

Given that the program that will be used in this work is the ANSYS program, which uses a roughness function that combines the characteristics of almost all roughness functions mentioned in the references so far for roughness with the modified basic wall law given by the following relation is used to incorporate the effects near the wall to simulate turbulent flow where the effect of wall roughness is most significant. Then, [29]:

$$\frac{U_p U^*}{\tau_w / \rho} = \frac{1}{k} \ln \left( E \frac{U^* y_p}{\mu} \right) - \Delta B \quad (9)$$

where  $U^* = C_\mu^{1/4} k^{1/2}$  and  $\Delta B = \frac{1}{k} \ln f_r U_p$  is the non-dimensional flow velocity along the wall in the boundary layer,  $U^*$  the friction velocity,  $\mu$  the dynamic viscosity,  $f_r$  is the roughness coefficient that determines the amount of interference due to roughness effects,  $\Delta B$  depends mainly on (type of sand, network nodes, ribs, ...) and the roughness size.

There isn't a particular roughness coefficient that corresponds to all different kinds of roughness, but  $\Delta B$  is related to the non-dimensional roughness height  $k_s^+$ , where  $k_s^+$  is the physical roughness height. It takes different forms:

- $k_s^+ \leq 2.25$  hydrodynamically smooth running
- $2.25 \leq k_s^+ \leq 90$  transitional flow
- $k_s^+ > 90$  completely rough region

According to numerical data, we find that the effects of roughness are very small in the hydrodynamically smooth system, but they are more important in the transitional system, and greatly affect the system with a completely rough region.

The previous three roughness regimes were split in ANSYS Fluent, and the formulas proposed by Cebeci and Bradshaw [33] using Nikuradse's data [25] were used to determine  $\Delta B$  for each regime as follows:

- For a hydrodynamically smooth system  $k_s^+ \leq 2.25$  and

$$\Delta B = 0$$

- For a transitional system  $2.25 \leq k_s^+ \leq 90$  and

$$\Delta B = \frac{1}{k} \ln \left[ \frac{k_s^+ - 2.25}{87.75} + C_s k_s^+ \right] \sin \left[ 0.4258 (\ln k_s^+ - 0.811) \right] \quad (10)$$

where  $C_s$  is the roughness constant (it is determined depending on the roughness type).

- For a system with absolute roughness  $k_s^+ > 90$  and

$$\Delta B = \frac{1}{k} \ln (1 + C_s k_s^+) \quad (11)$$

The logarithmic velocity profile is shown by the downward slope in Fig. 3 below:

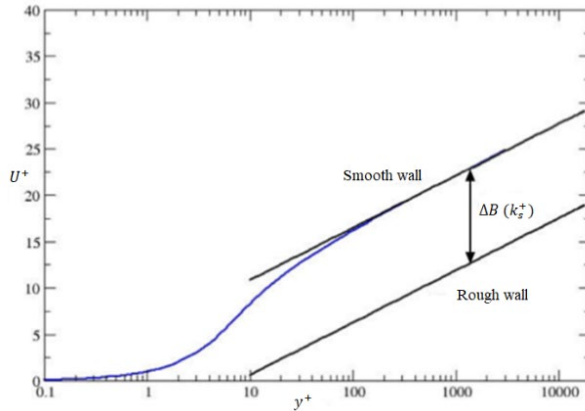


Figure 3

Downward regression of the logarithmic velocity profile [29]

Using ANSYS Fluent, multiple techniques can be employed depending on the disturbance model and near-wall processing to circumvent this issue, namely [29]:

1. Roughness height reduction as  $y^+$  decreases. This method is to redefine the roughness height based on network optimization.

$$k_s^+ = \min(k_s^+, y^+) \quad (12)$$

This ensures that as  $y^+$  approaches zero,  $k_s^+$  approaches zero as well. Therefore, the grid requirement for the rough walls in this case is  $y^+ > k_s^+$  in order to ensure the full effect of the roughness on the runoff.

2. Physical change of the wall. The second approach is based on the finding that the viscosity effect region is exclusively restricted to areas near smooth walls.

The viscosity region in the rough flow is destroyed and the viscosity effects are minimal in the transitional roughness regime, when the roughness elements are somewhat thicker than the sublayer and start to impede it.

The second method (physical change of the wall) is a default treatment for rough walls in all  $\omega$ -equation-based disorder models and the following  $\varepsilon$ -equation-based disorder models.

- Standard models, RNG, and the applicable k- $\varepsilon$  model
- Reynolds stress models

When using regular wall functions and scalable wall functions, this method can be applied. More scalable wall functions can be used than regular wall functions. Other coarse wall models do not require specific calibration for fine meshes, such as the Spalart-Allmaras model. Therefore, the first method is used (decrease in roughness height as  $y^+$  decreases).

### 3 Geometric Model and Boundary Conditions

The KVLCC2 ship model (the well-known KRISO Very Large Crude Carrier no. 2 model) was chosen for the calculations due to the abundance of experimental data. Since our study was performed at a low Froude number  $F_r = 0.142$ , space is missing the effect of free surface deformations was ignored.

Knowing that Froude number, a non-dimensional number, is a cross-sectional flow characteristic defined as the following relation:

$$F_r = \frac{v_{ship}}{gL_{wl}}$$

where  $v_{ship}$  : ship velocity ( $m \cdot s^{-1}$ ),  $g$  : acceleration of gravity ( $m \cdot s^{-2}$ ), and  $L_{wl}$  : length of the water line ( $m$ )

For assessing the mathematical equations and models pertinent to the standard case, a plate possessing analogous properties to the one employed in Schultz experiment [31] was specifically chosen.

### 3.1 Geometrical Dimensions and Boundary Conditions for the KVLCC2 Tanker Model

The essential geometric measurements of the KVLCC2 model are contrasted with those of the original ship in the accompanying table. The reduction ratio is  $\lambda = 58$

Table 1 shows the dimensions of the KVLCC2 ship and its model and, Fig.4 shows the CAD model of KVLCC2 [30].

Table 1  
The dimensions of the KVLCC2 ship and its model

Geometric dimension	Symbol	Full-scale KVLCC2	Model KVLCC2	Unit
Length between perpendiculars	$L_{pp}$	320	5.5172	$m$
Breadth (molded)	$B_{molded}$	58	1	$m$
Draft (molded)	$T$	20.8	0.3586	$m$
Blockage coefficient	$C_b$	0.8	0.8098	-
Wetted surface area without appendages	$S$	27194	8.0838	$m^2$
Displacement	$V$	312622	1.6023	$m^3$

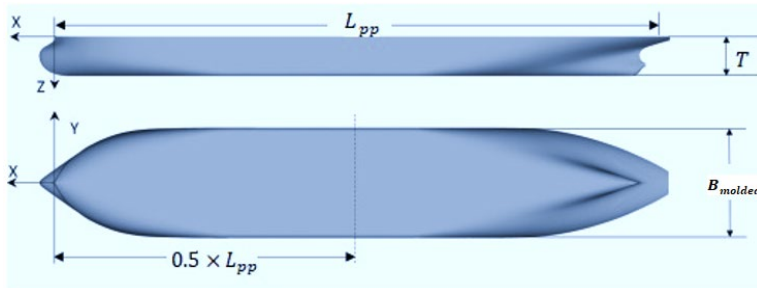


Figure 4  
Carrier ship model [30]

Figure 5 shows the boundary conditions and ship location in the test channel, as follows:

$$L' \times B' \times T' = 4.615L_{pp} \times 2.885L_{pp} \times 1.5L_{pp}$$

where  $L', B', T'$  are the length, width, and height of the geometric domains for the ship.

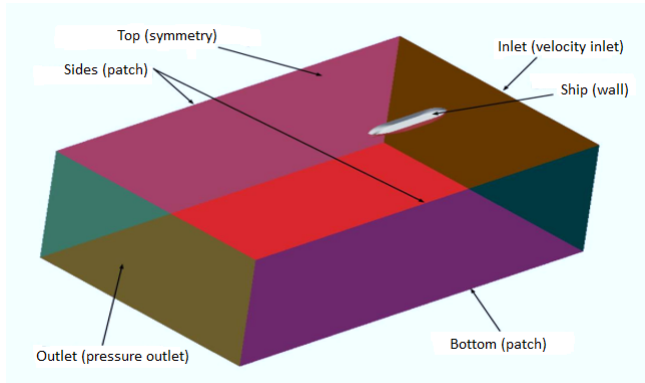


Figure 5

The boundary conditions around the ship

The ship is fixed and the fluid is moved at the same speed as the ship, achieving the Reynolds number, at which the vessel operates. The fluid inlet is the Inlet surface, and the outlet is the Outlet surface. The density is  $998.2 \text{ kg/m}^3$ , the viscosity is  $0.001003 \text{ kg/m}^{-4}$  and the ratio of specific heat is 1.4.

### 3.2 Geometrical Dimensions and Boundary Conditions for the Plate

Regarding the calibration plate, Table 2 shows the dimensions of Schultz plate and Fig. 6 shows it [31].

Table 2

The dimensions of the plate [31]

Geometric dimension	Symbol	Value	Unit
Length	$L_{plate}$	1.52	$m$
Breadth	$B_{plate}$	590	$mm$
Hight	$T_{plate}$	3.2	$mm$
Edge turning radius	$r_{plate}$	1.6	$mm$

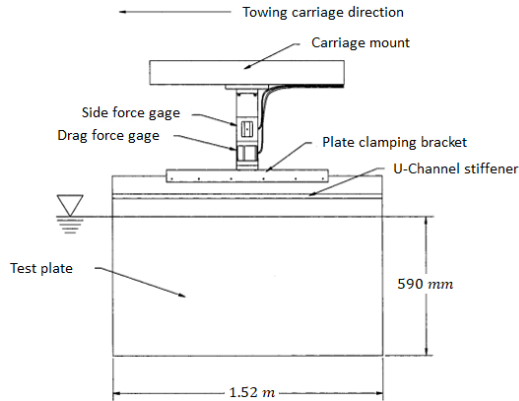


Figure 6  
Validation plate [31]

Figure 7 illustrates the geometric domain used in the case of the plate has the geometric dimensions defined according to Schultz's experiment [31] as follows:

$$L \times B \times T = 6L_{plate} \times 1.5L_{plate} \times 3.5L_{plate}$$

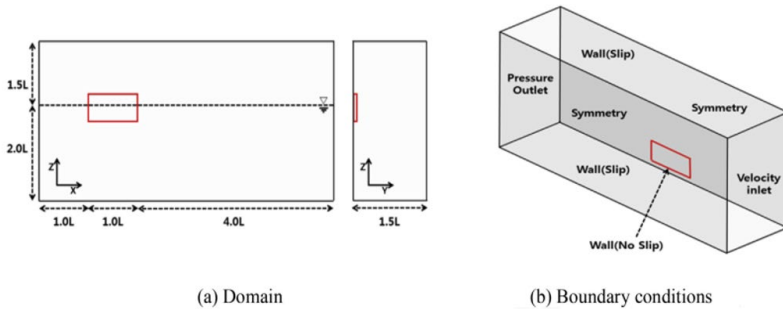


Figure 7  
Computational domain and boundary conditions around the plate

## 4 The Fluid Flow Model

The Navier-Stokes equations and the conservation of mass equation explain the motion of incompressible Newtonian fluids. Turbulence and flow are described by four equations. Using CFD and ANSYS 15, solutions to the system of equations were obtained.

Menter [32] put forth the  $k-\omega$  SST (SST-Shear Stress Transport) model. The  $k-\omega$  and  $k-\epsilon$  models are combined.

In this model, the benefits of the two models are integrated. While the  $k$ - $\varepsilon$  model is utilized outside the boundary layer region in the free-flow area, the  $k$ - $\omega$  model is applied close to the wall within the boundary layer region. The following are the transfer equations for the disturbance rate  $\omega$  and the disturbed kinetic energy  $k$  [32-36]:

-  **$k$  – equation**

$$\frac{\partial k}{\partial t} + u_j \frac{\partial k}{\partial x_j} = P_k - \beta^* k \omega + \frac{\partial}{\partial x_j} \left[ (v + \sigma_k v_T) \frac{\partial k}{\partial x_j} \right], i, j = 1, 2, 3, \dots \quad (13)$$

-  **$\omega$  – equation**

$$\frac{\partial \omega}{\partial t} + u_j \frac{\partial \omega}{\partial x_j} = \alpha S^2 - \beta \omega^2 + \frac{\partial}{\partial x_j} \left[ (v + \sigma_\omega v_T) \frac{\partial \omega}{\partial x_j} \right] + 2(1 - F_1) \sigma_{\omega 2} \frac{1}{\omega} \frac{\partial k}{\partial x_i} \frac{\partial \omega}{\partial x_i} \quad (14)$$

- **Eddy viscosity  $\mu_t$  -equation:**

$$\mu_t = \frac{\rho \alpha_1 k}{\max(\alpha_1 \omega, SF_2)}, S \frac{\partial u}{\partial y'} \quad (15)$$

$$F_1 = \tanh \left\{ \left[ \min \left[ \max \left( \frac{\sqrt{k}}{\beta^* \omega}, \frac{500\nu}{y^2 \omega} \right), \frac{4\sigma_{\omega 2} k}{CD_{k\omega} y^2} \right] \right]^4 \right\},$$

$$F_2 = \tanh \left[ \left[ \max \left( \frac{\sqrt{k}}{\beta^* \omega y}, \frac{500\nu}{y^2 \omega} \right) \right]^2 \right], \quad (16)$$

$$P_k = \min \left( \tau_{ij} \frac{\partial u_i}{\partial x_j}, 10\beta^* k \omega \right),$$

$$CD_{k\omega} = \max \left( 2\rho\sigma_{\omega 2} \frac{1}{\omega} \frac{\partial k}{\partial x_i} \frac{\partial \omega}{\partial x_i}, 10^{-10} \right).$$

The blending function is used to change between the two turbulence models. The model coefficients are presented in the following Table 3.

Table 3  
Coefficients of  $k$ - $\omega$  SST model [37]

$\beta^*$	$\alpha_2$	$\beta_1$	$\sigma_{k1}$	$\sigma_{k2}$	$\sigma_{\omega 1}$	$\alpha_2$	$\beta_2$	$\sigma_{\omega 2}$
0.09	0.555	0.075	0.85	1	0.5	0.44	0.0828	0.856

## 5 Mesh Generation

Figure 8 shows the structured grid employed in the numerical simulation, which was designed approximately with 482576 nodes in the case of a symmetric configuration. This grid was generated using ICEM program and was specifically oriented perpendicular to the ship's surface to ensure an accurate representation of the viscous flow field surrounding the ship. In terms of cell distribution, the bow, stern, and run sections of the ship were assigned a higher cell count compared to the central section. The minimum size of a cell ranged to be  $2.1078 \times e^{-10} m^3$  to  $4.0556 \times e^{-10} m^3$ , depending on the inflow velocity. This varying cell size enabled finer resolution in regions of higher flow complexity and facilitated capturing the relevant flow physics with greater fidelity.

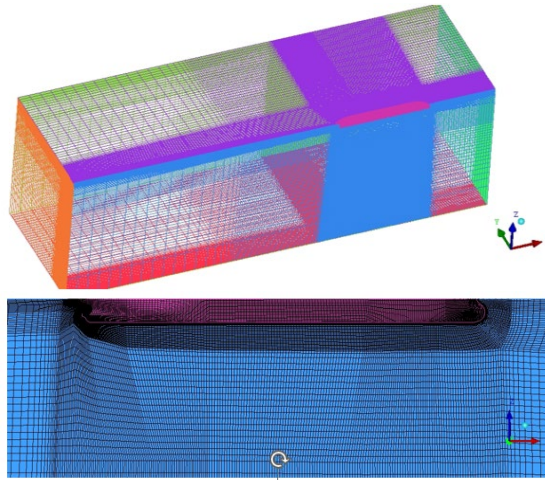


Figure 8

Structured grid around the KVLCC2 carrier (upper figure) and the refinement in the boundary layer region (lower figure)

The structured grid utilized in the numerical simulation of the calibration plate is shown in Fig. 9.

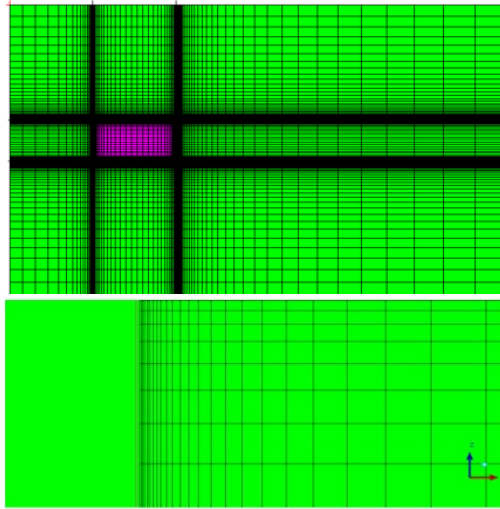


Figure 9

Structured grid around the plate (upper figure) and the refinement in the boundary layer region (lower figure)

This grid, designed for symmetric configuration, consisted of 1187640 nodes. The grid generation process was carried out using the ICEM program. To capture the flow characteristics near the plate surface accurately, a growth rate of 1.2 was chosen for grid refinement in the boundary layer region (see Fig. 9). This refinement strategy allowed for a more refined mesh resolution in the vicinity of the plate, ensuring enhanced fidelity in capturing near-wall flow phenomena. The structured nature of the grid facilitated efficient computational performance and maintained grid regularity, aiding in convergence and overall solution accuracy.

## 6 Solution Method

In our study, the finite element method (FEM) implemented within ANSYS serves as the primary numerical approach for accurately approximating the behaviour of our system.

To solve the continuity and momentum equations simultaneously for pressure and velocity instead of resorting to a pressure correction approach, coupled solver, with a Pressure-Based type, was implemented (which is a mix between a simple scheme and a PISO scheme). In terms of spatial discretization, least squares cell-based was chosen for the gradient and considered the pressure and the momentum as a second-order upwind while turbulent kinetic energy and specific dissipation ratio were considered as a first-order upwind.

The simulation was run under a steady-state setting, implying that the solution remains constant over time. The flow variables were also effectively and precisely initialized using the Hybrid initialization approach.

For the plate analysis, the pressure-velocity scheme was employed in conjunction with compressive volume fractions. To capture the gradient, a least squares cell-based approach was adopted, with a focus on - PRESTO! - pressure. As for the momentum, turbulent kinetic energy, and specific dissipation ratio, a second-order upwind scheme was utilized in a steady-state setting.

## 7 Validation Study

### 7.1 Assessment of Numerical Results for the Plate

The roughness function employed in ANSYS is currently undergoing study and development. Therefore, it is necessary to initially test this function on a standard case to ensure the reliability and accuracy of the results [31].

A comparison between the numerical and experimental results for plate total resistance coefficient  $C_T$ , considering various roughness height values ( $d$ ), is presented in Table 4. The experimental analysis involved testing the plate at two Froude numbers ( $F_r$ ). The results indicate that the error rate increases with higher Froude numbers and roughness heights.

KVLCC2 operates at a significantly lower Froude number of 0.142 [30] compared to the values listed in Table 4. Therefore, it is anticipated that the results will be even more accurate in this specific case.

Table 4  
Comparison between EFD and CFD (Present) of total resistance coefficient

Velocity ( $m.s^{-1}$ )	$F_r$	$d$ ( $\mu m$ )	$C_{T,EFD}$	$C_{T,CFD}$	Error %
2.0	0.518	0	0.003605	0.00359	0.4
		85	0.003663	0.00377	3.1
		129	0.003783	0.00397	5.1
3.8	0.984	0	0.003226	0.00320	0.8
		85	0.003423	0.00353	3.3
		129	0.003500	0.00369	5.4

It is observed that the maximum difference between the outcomes is 5.4% at a Froude number of 0.984 and a roughness height of 129  $\mu m$ . This disparity is considered highly acceptable. Thus, it can be concluded that when employing the

conditions (roughness function, RANS equations, and the  $k - \omega$  SST numerical model) for studying plate resistance, the results exhibit consistent agreement with the experimental data, both quantitatively and qualitatively. Consequently, these conditions were considered suitable for the vessel's circumstances and were implemented in the subsequent stage of analyzing KVLCC2.

## 7.2 Assessment of Numerical Results for KVLCC2

The experimental value ( $C_{T,EFD}$ ) of the total ship resistance coefficient for the KVLCC2 ship is available at Froude number 0.142 [30]. Considering that the total resistance coefficient defined in the relationship,

$$C_T = C_d + C_w,$$

where  $C_d$  is drag coefficient (the sum friction coefficient  $C_f$  and the pressure coefficient  $\tau_w$ ), and  $C_w$  is wave resistance coefficient. Since the Froude number is relatively small then the resistance of waves is neglected and drag resistance is dominated.

Table 5 illustrates the comparison between the results of EFD and CFD (obtained by ANSYS) for the total resistance coefficient.

Table 5  
Comparison between EFD and CFD (Present) of total resistance coefficient.

Velocity ( $m.s^{-1}$ )	$F_r$	$C_{T,EFD}$	$C_{T,CFD}$	Error %
1.047	0.142	0.00411	0.00394	4.1

Error percentage is calculated by the following relationship,

$$\frac{C_{T,EFD} - C_{T,CFD}}{C_{T,EFD}} \times 100.$$

The relative error 4.1%, refers to a convincing agreement between the experimental and numerical results.

## 8 Numerical Results and Discussion

The surface roughness of the hull has a notable impact on the propeller plane. When the hull surface is rough, it introduces disturbances and irregularities in the flow around the ship, particularly in the vicinity of the propeller.

These surface irregularities can lead to the formation of turbulent boundary layers and vortices in the flow. As the flow encounters these disturbances, it interacts with the propeller plane, causing several significant effects on velocity, pressure, kinetic energy, and vortex formation.

In this section, the surface roughness is defined by Eqs. (3) and (4), which applied in the numerical solution of Eqs. (5) and (6), in addition to the mass and momentum conservation laws.

## 8.1 The Effect of Surface Roughness on the Kinetic Field

Figure 10 illustrates how the velocity field changed in the area where propellers were being used. The changes of the velocity field in the propeller working area, where we clearly notice how with the increase in surface roughness the area of slow flow increases within the range  $(0-0.2 \text{ m.s}^{-1})$  and the flow direction perpendicular to the velocity gradient increases (the direction perpendicular to the symmetry plane). This means that the inconsistency in the flow in the propeller disc plane will increase with the increase in roughness, and this will inevitably lead to an increase in the oscillations around the propeller, which in turn will be transmitted to the stern of the ship and its hull.

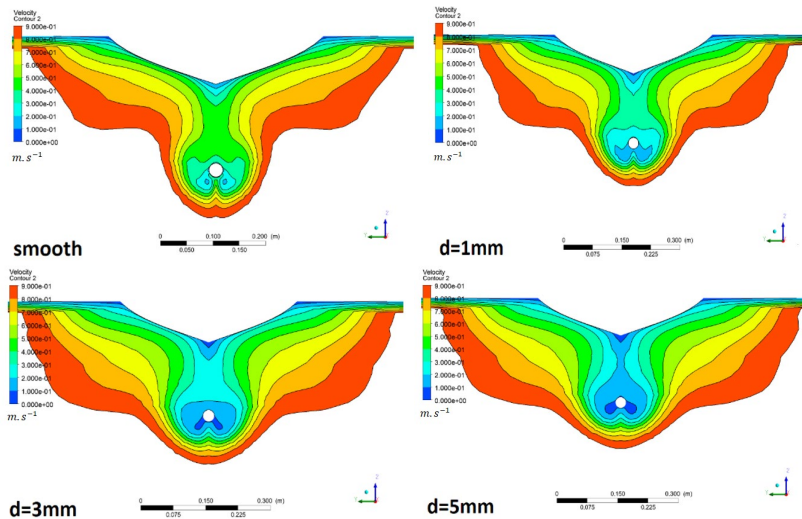


Figure 10

The changes of the velocity field according to the surface roughness in propeller plane for  $d = \text{smooth}, 1, 3, 5 \text{ mm}$

The increase in slow-flow regions within the propeller working area can affect the thrust generated by the propellers. where the presence of slow-flow areas can reduce the efficiency of the propellers, resulting in lower thrust production. This can potentially impact the overall performance and manoeuvrability of the ship.

Furthermore, the changes in flow direction perpendicular to the velocity gradient can affect the drag experienced by the ship's hull, where the increase in roughness can lead to an irregular flow pattern, resulting in higher drag forces acting on the hull. The drag force can hinder the forward movement of the ship, requiring more power to overcome the resistance and maintain desired speeds.

## 8.2 The Effect of Surface Roughness on the Kinetic Field

Figure 11 shows the change of the kinetic energy field according to the surface roughness in the working plane of the propeller. As we notice from this figure, with the increase in roughness, the kinetic energy gradient increases in the perpendicular direction to the plane of symmetry, and the value of kinetic energy increases in the propeller disc circle, and this indicates an increase in the intensity of the vortices entering the propeller disc, as we know in the case of bulk vessels and transport vessels. The lower part of the stern takes the form of a tube and accordingly, we have two huge vortices that enter into the plane of the propeller.

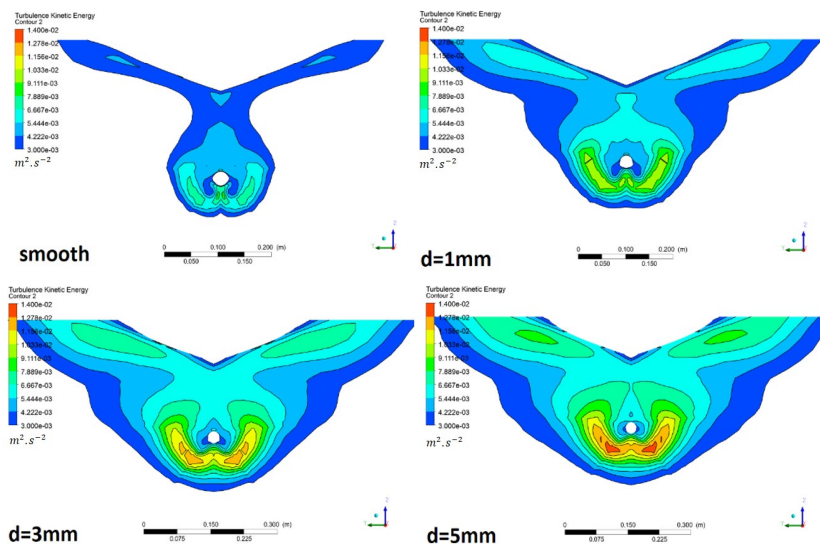


Figure 11

The changes of the kinetic energy field according to the surface roughness in propeller plane for  $d =$  smooth, 1, 3, 5 mm

## 8.3 The Effect of Surface Roughness on the Formation of Vortices

As shown in Fig.12, behind the hull of the studied ship, there are two large longitudinal vortices (A), in addition to two small vortices at the surface (B), and two small vortices at the propeller axis installation area (C). The eddies at the

surface are greatly influenced by the free surface and waves that form during sailing. The most important and influential vortices are the two huge vortices (A) because they enter directly into the propeller working area. These huge eddies form behind the tubular part of tankers and bulk carriers.

Accordingly, the intrusion of vortices into the propeller plane triggers a cascade of negative consequences that impact both the propeller system and overall fuel efficiency.

First, the presence of vortices induces heightened propeller vibrations, which can lead to mechanical instabilities and potential damage to the propeller structure. These vibrations not only compromise the structural integrity but also contribute to decreased thrust generation.

Second, the stresses exerted on the propeller blades increase because of the vortices interacting with the propeller. These elevated stresses can lead to premature fatigue and wear of the propeller blades, further impairing their performance and reducing the thrust force generated. The reduced thrust force necessitates higher power consumption to maintain desired speeds and propel the ship effectively.

Moreover, the disturbances caused by the vortices disrupt the smooth flow patterns and increase drag around the propeller, leading to an overall decrease in propulsion efficiency. This inefficiency translates into increased fuel consumption as more power is required to overcome the resistance and maintain the desired propulsion performance.

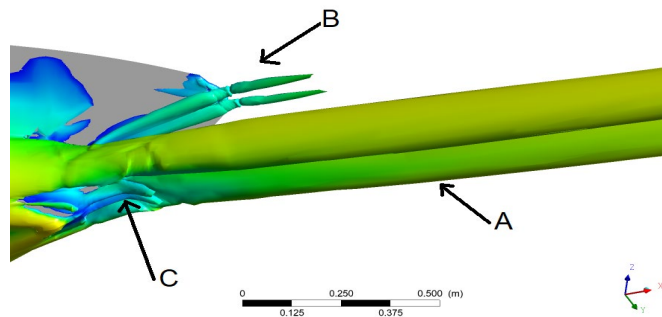


Figure 12

Vortices forming behind the hull of the KVLCC2 tanker

## Conclusions

In this research, the CFD technique was used to investigate the effect of surface roughness on vehicle resistance, and the following conclusions were reached:

- Propeller performance is significantly affected by the surface roughness of the hull.

- As the surface roughness of the hull increases, the velocity field in the working area of the propeller becomes more inconsistent, and the velocity gradient increases in the direction perpendicular to the flow. This leads to an increase in vibration in the propeller, which can negatively affect propeller performance and cause increased vibration and stress on the propeller blades.
- As the surface roughness increases, the kinetic energy gradient in the direction perpendicular to the plane of symmetry also increases. This results in an increase in the intensity of vortices entering the propeller, which can further degrade the performance of the propeller.
- When designing and calculating a vessel, it is essential to take surface roughness into account as it affects the performance of the propeller.
- An increase in surface roughness leads to an increase in velocity field inconsistency, kinetic energy, and vortex formation, which in turn can negatively affect propeller performance.
- RANS equations, k- $\omega$  SST model, and the roughness function used in the Ansys program give very good results in marine applications and help save material costs and time, especially when calculating resistances.
- Roughness has a significant impact on the forces acting on the vessel and the flow characteristics around the hull.
- An increase in surface roughness leads to an increase in velocity field inconsistency, kinetic energy, and vortex formation, which in turn can negatively affect propeller performance.
- These results are useful for predicting the energy required to operate the ship in marine conditions, fuel consumption, and greenhouse gas emissions.

## Nomenclature

### Symbols

$B$	-	constant considers the effect of surface roughness on the velocity distribution
$B_{molded}$	$m$	breadth (molded)
$B_{plate}$	$mm$	breadth of the plate
$B'$	$m$	width of the geometric domain for the ship model
$B''$	$m$	width of the geometric domain for the plate
$C_b$	-	blockage coefficient
$C_d$	-	drag coefficient
$C_f$	-	friction coefficient

$C_p$	-	pressure coefficient
$C_s$	-	roughness constant
$C_T$	-	total resistance coefficient
$C_{T,EFD}$	-	total resistance coefficient according to experimental results
$C_{T,CFD}$	-	total resistance coefficient according to numerical results
$C_w$	-	wave resistance coefficient
$d$	$m$	roughness height value
$f_r$	-	roughness coefficient
$F_r$	-	Froude number
$g$	$m.s^{-2}$	acceleration of gravity
$h$	$m$	the characteristic linear dimension
$k_{const}$	-	Kármán's constant
$k$	$m$	roughness height
$k_s$	$m$	the equivalent sand roughness height (physical roughness height)
$k_s^+$	-	non-dimensional roughness height
$L_{plate}$	$m$	length of the plate
$L_{pp}$	$m$	length between perpendiculars
$L'$	$m$	length of the geometric domain for the ship model
$L''$	$m$	length of the geometric domain for the plate
$L_{wl}$	$m$	length of the water line
$p$	$N/m^2$	pressure
Re	-	Reynolds number
$r_{plate}$	$mm$	edge turning radius for the plate
$S$	$m^2$	wetted surface area without appendages
$T$	$m$	draft (molded)
$T_{plate}$	$mm$	draft of the plate
$T'$	$m$	draft of the geometric domain for the ship model
$T''$	$m$	draft of the geometric domain for the plate

$U$	$m.s^{-1}$	the mean velocity of the object relative to the fluid
$U_e$	$m.s^{-1}$	the free flow velocity
$U_p$	-	the non-dimensional flow velocity along the wall in the boundary layer
$U^+$	-	the non-dimensional velocity in the boundary layer (velocity profile)
$U^*$	$m.s^{-1}$	friction velocity
$U_\tau$	$m.s^{-1}$	frictional velocity
$\Delta U^+$	-	roughness function
$V$	$m^3$	displacement
$y$	$m$	wall distance
$y^+$	-	the non-dimensional distance measured perpendicularly to the surface

### Greek letters

$\alpha, \beta$	-	$k-\omega$ SST coefficients
$\delta$	$m$	the boundary layer thickness
$\varepsilon$	-	the rate of dissipation of the turbulent kinetic energy
$\mu$	$kg/ms$	dynamic viscosity
$\mu_t$	$kg/ms$	Eddy viscosity
$\nu$	$m^2/s$	kinematic viscosity
$\nu_{ship}$	$m.s^{-1}$	ship velocity
$\nu_T$	$m^2/s$	turbulent viscosity
$\rho$	$kg/m^3$	the density of the fluid
$\sigma$	$N/m^2$	normal stress
$\tau_w$	$N/m^2$	shear stress
$\omega$	$1/S$	specific dissipation rate

### Acknowledgement

The first author was supported by Dr. Nawar Abbas, Assistant Dr-Eng at Marine Engineering Department, Faculty of Mechanical and Electrical Engineering, Tishreen University, Latakia, Syria. The authors were supported by project no. 129257 implemented with the support provided to the corresponding author from the National Research, Development and Innovation Fund of Hungary, financed under the K18 funding scheme.

## References

- [1] H. Schlichting, K. Gersten: "Boundary layer theory". New York, USA: Springer- Verlag Berlin Heidelberg, 2000. 1960
- [2] J. D. Anderson: "Ludwig Prandtl's boundary layer," *Physics Today*, vol. 58, no. 12, pp. 42-48. December, 2005, doi: 10.1063/1.2169443
- [3] S. Song, Y.K. Demirel, C. De Marco Muscat-Fenech, D. Sant, T.; Villa, T. Tezdogan, A. Incecik: "Investigating the Effect of Heterogeneous Hull Roughness on Ship Resistance Using CFD". *J. Mar. Sci. Eng.*, vol. 9, no. 2, pp. 202. 2021, <https://doi.org/10.3390/jmse9020202>
- [4] S. Song, R. Ravenna, S. Dai, C. De Marco Muscat-Fenech, G. Tani, Y.K. Demirel, M. Atlar, S. Day, A. Incecik: "Ex-perimental investigation on the effect of heterogeneous hull roughness on ship resistance". *Ocean Eng.*, vol. 223, p. 108590. 2021
- [5] S. Song, Y.K. Demirel, M. Atlar, S. Dai, S. Day, O. Turan: "Validation of the CFD approach for modelling roughness effect on ship resistance". *Ocean Eng.*, vol. 200, p. 107029. 2020, doi: 10.1016/j.oceaneng.2020.107029
- [6] Y. Tahara, J. Ando: " Comparison of CFD and EFD for KCS container ship in without/with propeller conditions ". In: *Gothenburg: A Workshop on Numerical Ship Hydrodynamics*. Chalmers University of Technology, Gothenburg, Sweden. 2000, vol. 192, pp. 63-70, doi: <https://doi.org/10.2534/jjasnaoe1968.2002.63>
- [7] S. B. Pope: "Turbulent Flows". UK, Cambridge University Press. 2000
- [8] H. Herwig: "Strömungsmechanik". Berlin, Heidelberg: Springer Berlin Heidelberg, pp. 3-11. 2002, doi: 10.1007/978-3-662-10107-0\_1
- [9] M. P. Schultz, G. W. Swain: "The influence of biofilms on skin friction drag," *Biofouling*, vol. 15, no. 1-3, pp. 129-139, May 2000, doi: 10.1080/08927010009386304
- [10] A. E. Perry, W. H. Schofield, P. N. Joubert: "Rough wall turbulent boundary layers," *J. Fluid Mech.*, Vol. 218, pp. 405-438. September 1990, doi: <https://doi.org/10.1017/S0022112090001057>
- [11] J. Nikuradse: "Laws of Flow in Rough Pipes", *Forschung auf dem Gebiete des Ingenieurwesens*. Ausgabe B Band 4, July/August, 1933, no.1292
- [12] M. A. Shockling, J. J. Allen, and A. J. Smits: "Roughness effects in turbulent pipe flow", *J. Fluid Mech.* 2006, doi: 10.1017/S0022112006001467
- [13] M. P. Schultz, K. A. Flack: "The rough-wall turbulent boundary layer from the hydraulically smooth to the fully rough regime", *J. Fluid Mech.*, vol. 580, pp. 381-405. 2007, doi: 10.1017/S0022112007005502
- [14] J. Nikuradse: "Laws of Flow in Rough Pipes," *J. Appl. Phys.*, 1950, doi: 10.1063/1.1715007

- [15] F. Hama: "Boundary-layer characteristics for smooth and rough surfaces", *Trans. - Soc. Nav. Archit. Mar. Eng.*, vol. 62, pp. 333-351. 1954, URL=<https://cir.nii.ac.jp/crid/1572824499659264512>
- [16] R. A. Antonia, R. E. Luxton: "The response of a turbulent boundary layer to a step change in surface roughness Part 1. Smooth to rough". *J. Fluid Mech.*, vol. 48, no. 4, pp. 721-761. 1971, doi: 10.1017/S0022112071001824
- [17] R. A. Antonia, R. E. Luxton: "The response of a turbulent boundary layer to a step change in surface roughness. Part 2. Rough-to-smooth," *J. Fluid Mech.*, vol. 53, no. 4, pp. 737-757. 1972, doi: 10.1017/S002211207200045X
- [18] P. M. Ligrani, R. J. Moffat: "Structure of transitionally rough and fully rough turbulent boundary layers," *J. Fluid Mech.*, vol. 162, pp. 69-98. 1986, doi: 10.1017/S0022112086001933
- [19] P. R. Bandyopadhyay: "Rough-Wall Turbulent Boundary Layers in the Transition Regime". *J. Fluid Mech.*, vol. 180, pp. 231-266. 1987, doi: 10.1017/S0022112087001794
- [20] P. A. Krogstad, R. A. Antonia, L. W. B. Browne: "Comparison between rough and smooth-wall turbulent boundary layers" *J. Fluid Mech.*, vol. 245, pp. 599-617. 1992, doi: 10.1017/S0022112092000594
- [21] M. Schultz: "The effect of biofilms on turbulent boundary layers," Ph.D. Thesis, Florida Institute of Technology. 1998
- [22] M. P. Schultz, G. W. Swain: "The effect of biofilms on turbulent boundary layers," *J. Fluids Eng. Trans. ASME*, 1999, doi: 10.1115/1.2822009
- [23] M. P. Schultz: "Effects of coating roughness and biofouling on ship resistance and powering", *Biofouling*, vol. 23, pp. 331-341. 2007, doi: 10.1080/08927010701461974
- [24] H. Schlichting: "Boundary layer theory: Seventh edition.," 1979
- [25] Nikuradse, J: "Laws of flow in rough pipes [English translation of *Stromungsgesetze in rauhen Rohren*]," *VDI-Forschungsheft*, vol. 361, pp. 1-22. 1930
- [26] Y. K. Demirel, M. Khorasanchi, O. Turan, A. Incecik: "A parametric study: Hull roughness effect on ship frictional resistance," *RINA, R. Inst. Nav. Archit. - Int. Conf. Mar. Coatings*, 2013
- [27] Y. K. Demirel, O. Turan, A. Incecik: "Predicting the effect of biofouling on ship resistance using CFD," *Appl. Ocean Res.* vol.6 2, pp. 100-118. 2017, doi: 10.1016/j.apor.2016.12.003
- [28] D. Owen, Y. K. Demirel, E. Oguz, T. Tezdogan, and A. Incecik: "Investigating the effect of biofouling on propeller characteristics using CFD," *Ocean Eng.* vol. 159, pp. 505-516, 2018, doi: 10.1016/j.oceaneng.2018.01.087

- [29] Ansys Fluent 2020 R1-Theory Guide, [https://ansyshelp.ansys.com/account/secured?returnurl=/Views/Secured/corp/v201/en/flu\\_th/flu\\_th.html?q=ansys%20fluent%20theory%20guide](https://ansyshelp.ansys.com/account/secured?returnurl=/Views/Secured/corp/v201/en/flu_th/flu_th.html?q=ansys%20fluent%20theory%20guide). 2020
- [30] “MOERI KVLCC2 Geometry and Conditions, SIMMAN 2008, FORCE Technology”  
[http://www.simman2008.dk/KVLCC/KVLCC2/kvlcc2\\$\\_geometry.html](http://www.simman2008.dk/KVLCC/KVLCC2/kvlcc2$_geometry.html)
- [31] M. P. Schultz: “Frictional resistance of antifouling coating systems,” *J. Fluids Eng. Trans. ASME*, vol. 126, no. 6, pp. 1039-1047. 2004, doi: 10.1115/1.1845552
- [32] F. R. Menter: “Two-equation eddy-viscosity turbulence models for engineering applications,” *AIAA J.*, vol. 32, no. 8, pp. 1598–1605, Aug. 1994, doi: 10.2514/3.12149
- [33] T. Cebeci, "Turbulence models and their application: efficient numerical methods with computer programs," Springer. vol. 24, no. 3, pp. 407. 2004, doi: 10.1016/j.euromechflu.2004.08.001
- [34] Hoch, Toralf: " Development of a "numerical test bench" for turbine wheel gas meters," Diss. Duisburg, Essen, Universität Duisburg-Essen, Diss. 2011
- [35] CFD Online, "*k- $\omega$*  SST model," [https://www.cfd-online.com/Wiki/SST\\_k-omega\\_model](https://www.cfd-online.com/Wiki/SST_k-omega_model), August, 2013
- [36] Wilcox D. C: "Turbulence modeling for CFD," DCW industries, La Canada, vol. 98, no. 980, pp. 405. 1993, doi:10.1017/S0001924000027032
- [37] Menter F. R., Kuntz M., and Langtry R: "Ten years of industrial experience with the SST turbulence model," *Turbulence, heat and mass transfer*, vol. 4, no. 1, pp. 625-632. 2003